Non-Griffiths-like cluster formation in the double-perovskite Gd_2CoMnO_6: Evidence from critical behavior

Moumita Das,[1] Prosenjit Sarkar,[2] and Prabhat Mandal[1]
[1]*Saha Institute of Nuclear Physics, HBNI, 1/AF Bidhannagar, Calcutta 700064, India*
[2]*Department of Physics, Serampore College, Serampore 712201, India*

(Received 10 September 2019; revised manuscript received 21 January 2020; accepted 7 April 2020; published 27 April 2020)

We have shown that ferromagnetic double perovskite Gd_2CoMnO_6 exhibits the characteristics of clustered phase, which are quite different from that of Griffiths phase observed in several perovskite compounds. The Yang-Lee theory of phase transition predicts that the essential singularity of the Griffiths phase leads to very unusual critical phenomena, including a discontinuity in the magnetization isotherm at $T = T_C$, which is reflected through the large value of critical exponent δ. However, the critical exponent δ for Gd_2CoMnO_6, determined from magnetization scaling analysis, comes out to be very small ($\delta = 1.55 \pm 0.03$). The small value of δ suggests that the continuous ordering is slow, indicating non-Griffiths-like cluster formation in the studied system, which is further supported by the evolution of susceptibility with temperature and magnetic field. Also, the observed values of all the three exponents β ($= 1.18 \pm 0.06$), γ ($= 0.65 \pm 0.01$), and δ are far from any existing universality class and they deviate from the mean-field values in the opposite direction to that for the conventional universality.

DOI: 10.1103/PhysRevB.101.144433

I. INTRODUCTION

Double perovskites $R_2MM'O_6$ (R: rare-earth ions or Y, La; M, M': transition metal ions) have attracted considerable research interest due to their various fascinating properties like multiferroicity [1–3], spin-phonon coupling [4–6], cationic ordering [7,8], colossal magnetoresistance [9], large magnetocapacitance, etc. [10,11]. These compounds crystallize either in monoclinic structure with $P2_1/n$ space group for ordered state or in the orthorhombic $Pbnm$ structure for disordered state [12]. Most of the ordered double perovskites exhibit ferromagnetism due to the superexchange interaction between the ordered M^{2+} and M'^{4+} ions [13]. Even in the ordered state itself, some of the M and M' cations interchange their crystallographic positions and introduce antisite disorder [4,14,15]. Such disorders instigate additional antiferromagnetic (AFM) interactions in the form of M^{2+}-O-M^{2+} or M'^{4+}-O-M'^{4+} and thus weaken the ferromagnetism.

There are several reports on magnetic and magnetodielectric properties of double perovskites R_2(Co/Ni)MnO_6, but the majority of them address La-based systems [1,2,10,16,17]. As R changes from La to Lu, the reduction of the size of the rare-earth element causes significant modification in Co-O-Mn/Ni-O-Mn bond angle and bond length and, as a consequence, the ferromagnetic (FM) transition temperature (T_C) decreases [18] and multiple magnetic interactions develop in the system, leading to an inhomogeneous magnetic ground state, as observed in several perovskite manganites in the form of clustered or phase separated states [4,14,19]. Among the various forms of clustered phases, the "Griffiths-like" phase has drawn more attention due to its interesting magnetic response. The formation of the Griffiths phase (GP) occurs below a characteristic temperature, called the Griffiths temperature (T_{GP}). For $T_C < T < T_{GP}$, the system is in an unusual magnetic state where the short-range FM clusters of different sizes exist [20–23]. In this narrow range of temperature, magnetic properties show several characteristics, such as (i) the inverse susceptibility (χ^{-1}) starts to deviate in downward direction from the linear Curie-Weiss behavior just below T_{GP}, as temperature approaches T_C from above, (ii) χ^{-1} follows a power-law behavior [20,23]

$$\chi^{-1}(T) = A\left(T - T_C^R\right)^{1-\lambda}, \tag{1}$$

where T_C^R is the critical temperature below which χ diverges and λ is an exponent such that $0 < \lambda < 1$ for $T_C^R < T < T_{GP}$ and $\lambda = 0$ for $T > T_{GP}$, and (iii) the downturn in χ^{-1} gradually suppresses with increasing field strength and eventually disappears [20,23].

In several magnetic systems, including perovskite-type manganites and cobaltites, the presence of GP has been experimentally verified [19,20,24]. The GP has also been reported in some double perovskites such as Tb_2NiMnO_6 [4], Pr_2CoMnO_6 [25], Ho_2NiMnO_6 [26], and Nd_2CoMnO_6 [27], etc., whereas Dy_2NiMnO_6 [28] and Lu_2NiMnO_6 [29] do not show GP-like behavior. The presence of the Griffiths-like clustered phase in the above mentioned compounds has been claimed solely from the downturn behavior of the $\chi^{-1}(T)$ curve slightly above the T_C [22]. However, this downturn in $\chi^{-1}(T)$ is not sufficient to claim the formation of GP in the temperature region $T_C < T < T_{GP}$. The analysis of critical behavior is one of the important techniques to confirm the GP formation [22,23,30]. In this work, we present the detailed analysis of critical behavior of ferromagnetic double

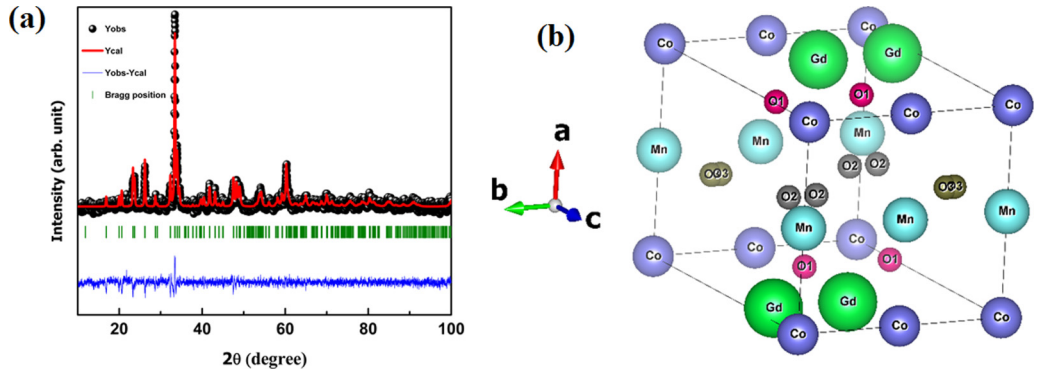

FIG. 1. (a) X-ray diffraction pattern of Gd_2CoMnO_6 (GCMO) and (b) the schematic crystal structure of GCMO.

perovskite Gd_2CoMnO_6 (GCMO). This is a scaling analysis in a double perovskite system to determine the nature of the clustered phase. The critical exponents β, γ, and δ, obtained through the scaling analysis of magnetization data and the magnetocaloric results, clearly demonstrate that the Griffiths-like phase is absent in the studied system. Moreover, the deduced values of the exponents are quite far from any known universality class.

II. EXPERIMENTAL DETAILS

The polycrystalline sample of GCMO was prepared by a conventional solid-state reaction method using high purity Gd_2O_3 (99.9%), Co_3O_4 (99.9%), and $MnCO_3$ (99.9%) powders [13]. Before use, Gd_2O_3 was preheated at 950 °C for 24 h. The starting materials were mixed thoroughly in an appropriate ratio, and heated at 1200 °C in air for a few days with intermediate grindings. Finally, the product was reground, pressed into pellets, and sintered at 1350 °C in air for 24 h. The phase purity and crystal structure of the samples have been determined by high-resolution x-ray powder diffraction with CuK_α radiation (Rigaku TTRAX II) ($\lambda = 1.5406$ Å) at room temperature. The experimental x-ray intensity profile along with the theoretical fit and the Bragg positions are shown in Fig. 1(a). All the peaks in the diffraction pattern can be indexed well with monoclinic unit cell having $P21/n$ crystallographic symmetry [31]. Within the x-ray resolution, we have not observed any peak due to the impurity phase. The lattice parameters determined from Rietveld analysis are $a = 5.467$, $b = 5.510$, and $c = 7.651$ Å with $\beta = 89.951°$, which are close to the previously reported values [31]. The schematic crystal structure of GCMO has been shown in Fig. 1(b).

A small piece of a rectangular shape sample of approximate dimensions $\sim 4 \times 0.5 \times 0.4$ mm^3 was cut from the polycrystalline pellet for dc magnetization (M) measurements in a 7 T SQUID-vibrating sample magnetometer (Quantum Design). The data for each isotherm were recorded in the field range of 0–7 T at different temperatures between 2 and 150 K and the temperature dependence of magnetization was measured in the range 1.8–390 K. To minimize the demagnetization effect, the magnetic field was applied along the longest dimension of the sample. For each isothermal magnetization measurement, the sample temperature was stabilized for 30 min. Data were collected for both increasing and decreasing fields. We did not observe any difference in $M(H)$ between increasing and decreasing fields above 114 K. Magnetization has been measured using two different protocols: (a) the field-cooled-cooling (FCC) magnetization and (b) the field-cooled-warming (FCW) magnetization. In the FCC cycle, the measurement was performed during the cooling process under applied magnetic field. In the FCW cycle, the sample was cooled down to lowest temperature in an applied magnetic field and the measurement was performed during the heating cycle. To check the saturation behavior, magnetization was measured at 2 K for fields up to 9 T in a physical property measurement system (Quantum Design). The heat capacity measurement was done in a physical property measurement system (Quantum Design) by relaxation method in the temperature range 5–300 K.

III. RESULTS AND DISCUSSION

A. Magnetization and heat capacity

Figure 2(a) shows the temperature dependence of FCC and FCW magnetization for GCMO at a field of 100 Oe. In the paramagnetic (PM) state, M increases slowly with decreasing temperature down to $\approx$ 123 K. However, M increases sharply below 123 K, indicating the onset of long-range FM ordering. With further decrease in T, M continues to increase like a Brillouin function down to $\sim$43 K, below which M starts to decrease. Similar behavior in $M(T)$ has also been observed in other double perovskite systems [13,14,31–33]. The decrease in M at low temperature has been attributed to complex interplay of magnetic interaction of Gd and Mn/Co sublattices [13,18,31,33]. Similar to the previous report a very weak thermal hysteresis has been observed between FCC and FCW magnetization cycles [34]. With the increase in magnetic field strength, the anomaly below 43 K progressively suppresses and M shows a sharp increase at low temperature for the field above 1 kOe, as shown in the upper inset of Fig. 2(a). This sharp increase in M is due to the contribution of a large PM moment of rare-earth Gd^{3+} ion, which aligns along the direction of field above a threshold value. The lower inset of Fig. 2(a) displays $M(H)$ hysteresis loops at low temperature well below T_C. Even at 2 K, we did not observe saturationlike behavior in the $M(H)$ curve at high field up to 9 T (not shown). At 2 K and 7 T, the value of magnetization is $16.6\mu_B$/f.u. The obtained value of M matches well with the previous reports [13,31]. The FM ordering temperature T_C, estimated from the $M(T)$ curve, is also confirmed through heat capacity (C_p)

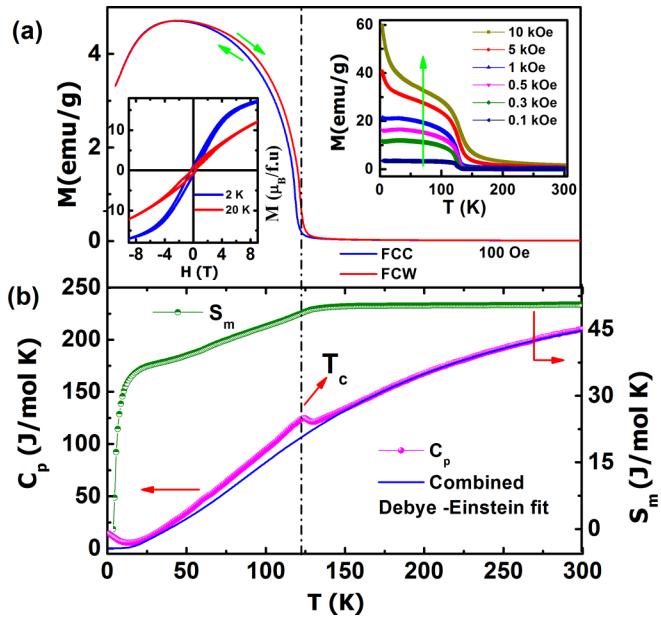

FIG. 2. (a) Main panel shows the temperature (T) dependence of magnetization (M) of GCMO at $H = 100$ Oe for both field-cooled-cooling (FCC) and field-cooled-warming (FCW) conditions. The upper inset shows $M(T)$ curves for different H where the arrow indicates the direction of increase of magnetic field strength. The lower inset displays $M(H)$ hysteresis loop at 2 and 20 K. (b) T dependence of heat capacity (C_p) along with the combined Debye-Einstein model fit (solid line) and magnetic entropy (S_m) of GCMO. The arrow indicates the transition temperature T_C.

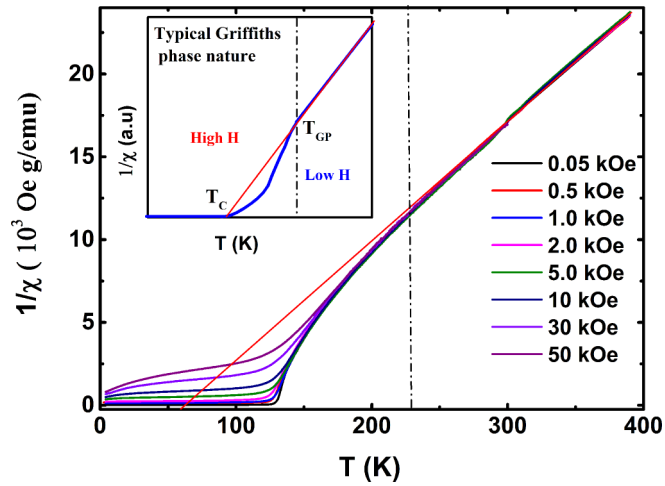

FIG. 3. Main panel shows the temperature dependence of inverse dc susceptibility ($\chi^{-1} = H/M$) of GCMO for different applied fields. The red line shows the linear fit to the Curie-Weiss law. The inset shows the expected nature of the Griffiths phase.

data as shown in Fig. 2(b), where a peak has been observed at around 123 K [31]. As expected, no anomaly is seen in the C_p curve at low temperature where M is observed to decrease. However, the $C_p(T)$ curve shows an upturn below ~20 K. Similar increase in C_p has also been reported earlier in single crystals of GCMO and other double perovskite compounds such as Tb_2CoMnO_6 [13,31,35] and attributed to the short-range AFM ordering of rare-earth moments. Thus this upturn in GCMO is due to the short-range AFM ordering of the Gd^{3+} moments. For understanding the nature of the FM phase transition, we have estimated the magnetic entropy (S_m) using the expression $S_m(T) = \int (\frac{C_m}{T})dT$, where C_m is the magnetic contribution to heat capacity and has been calculated by subtracting the lattice part from the total heat capacity. The lattice heat capacity has been calculated using the combined Debye-Einstein model [36]. The variation of S_m with T is shown in Fig. 2(b). The continuous change in $S_m(T)$ around T_C indicates that the FM transition is second order in nature.

B. Magnetic susceptibility

The main panel of Fig. 3 presents the temperature dependence of inverse dc susceptibility, χ^{-1} ($=H/M$), for various applied fields. At high temperature above ~250 K, χ^{-1} increases almost linearly with T. However, below 250 K, χ^{-1} starts to deviate from the linear behavior and shows a downward curvature. Often, this faster decrease of χ^{-1} in the PM state has been attributed to the formation of short-range FM clusters [20,22,23,30]. To check whether the clustered phase has the characteristics of GP, the T dependence of χ below T_{GP} has been analyzed in detail. We observe that $\chi^{-1}(T)$ does not follow the power-law expression, as described in Eq. (1), suggesting that the clustered phase is not Griffiths-like. For the accurate determination of T_C^R and λ in GP, T_C^R should be varied in such a way so that λ becomes zero for $T > T_{GP}$ [20]. This criterion suggests that T_C^R should be very close to the temperature obtained by extrapolation of the high temperature linear part of $\chi^{-1}(T)$ to zero. In compounds where GP is observed, T_C^R is found to be slightly higher than T_C [20,26]. However, the T_C^R (≈ 75 K) in GCMO is much lower than T_C (≈ 123 K), not consistent with the behavior expected for GP. For further confirmation of the nature of clustered phase, we have examined the effect of the magnetic field on $\chi^{-1}(T)$, which is displayed in Fig. 3. In the case of GP, the downturn in $\chi^{-1}(T)$ curve gradually weakens with increasing field strength and disappears at high field, as shown schematically in the inset of Fig. 3 [20,22,23,30]. On the other hand, for GCMO, the downturn in χ^{-1} does not suppress even under application of magnetic field as high as 50 kOe. This kind of field dependence of χ^{-1} indicates "non-Griffiths-like" nature of the clustered phase [37].

The downward curvature in inverse susceptibility versus temperature plot (Fig. 3) suggests that both rare-earth (Gd^{3+}) and transition metal ion (Co^{2+}/Mn^{4+}) sublattices contribute to the total susceptibility. Hence we have used the modified Curie Weiss (CW) expression to incorporate the contribution of the individual sublattice to the total magnetic susceptibility,

$$\chi(T) = \chi_{RE} + \chi_{TM} = \frac{C_{RE}}{T} + \frac{C_{TM}}{T - \Theta_{TM}}, \qquad (2)$$

where C_{RE} and C_{TM} are the Curie constants of the rare-earth and transition metal ion sublattices, respectively, whereas the Θ_{TM} is the CW temperature for the Co^{2+}/Mn^{4+} sublattice. The subscripts RE and TM denote the parameters for rare-earth Gd^{3+} and transition metal sublattices, respectively. As Gd^{3+} moments do not show any long-range ordering down to 2 K, we have used CW temperature $\Theta_{RE} = 0$. Also, the Curie

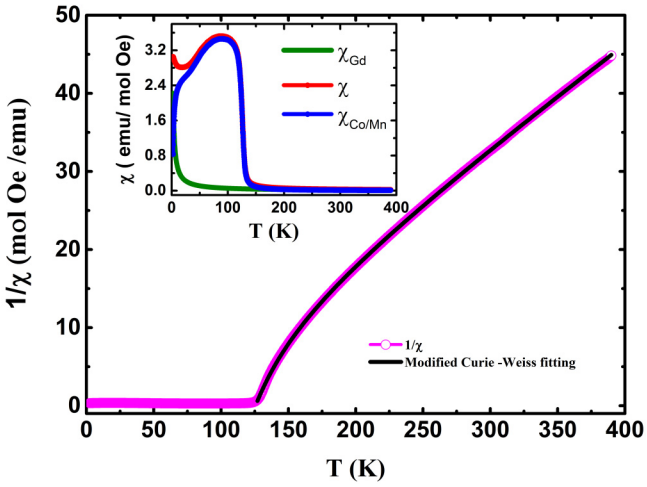

FIG. 4. Main panel shows the temperature dependence of inverse dc susceptibility ($\chi^{-1} = H/M$) of GCMO at $H = 500$ Oe. The blue curve shows the modified Curie-Weiss fitting and the inset shows the contribution of the χ_{Gd} and $\chi_{Co/Mn}$ to the total experimental susceptibility χ.

constant C_{RE} for the Gd sublattice was calculated using the theoretical value of effective paramagnetic moment $\mu_{eff} = 15.8\mu_B$/f.u. and the Landé g factor $g = 2$. The measured susceptibility has been fitted with Eq. (2) and shown in Fig. 4. It is clear from the figure that experimental data can be fitted with Eq. (2) over a wide temperature range. In this context, we would like to mention that a similar type of fit has been used for GCMO and other compounds where both rare-earth and transition metal sublattices are present [26,38,39]. The fit yields $\Theta_{TM} = 125.3$ K, which is close to T_C, and the effective paramagnetic moment of the Co^{2+}/Mn^{4+} sublattice is $5.4\mu_B$/f.u., which is close to the theoretical value [38]. The contribution of each sublattice to the total susceptibility has also been plotted in the inset of Fig. 4. The plots show that the contribution of χ_{TM} is significantly larger as compared to χ_{RE} when T approaches T_C, i.e., in the the critical region. For example, $\chi_{TM} = 2.9$ emu/mol Oe and $\chi_{RE} = 0.046$ emu/mol Oe at 120 K. However, at low temperature where χ shows a sharp increase with decreasing temperature, Gd^{3+} moment dominates magnetic susceptibility. We have also calculated the contribution to magnetization due to the Gd moment using the relation $M_{Gd} = \chi_{RE}H$ and it is found that the value of the Gd^{3+} moment is less than 1% of the total moment in the critical region.

C. Field-induced metamagnetic transition

From the temperature and magnetic field dependence of magnetization and susceptibility, several groups reported multiple magnetic phase transitions in GCMO [33,34,40]. GCMO exhibits complex magnetic behavior due to strong competition between rare-earth and transition metal sublattices which is yet to be understood. Also, some of the reported features such as metamagnetic transition and spin-glass behavior [34,40,41] appear to be sensitive, to some extent, to sample quality. For this reason, we have recorded the $M(H)$ loop at different temperatures using our highly sensitive SQUID-VSM facility.

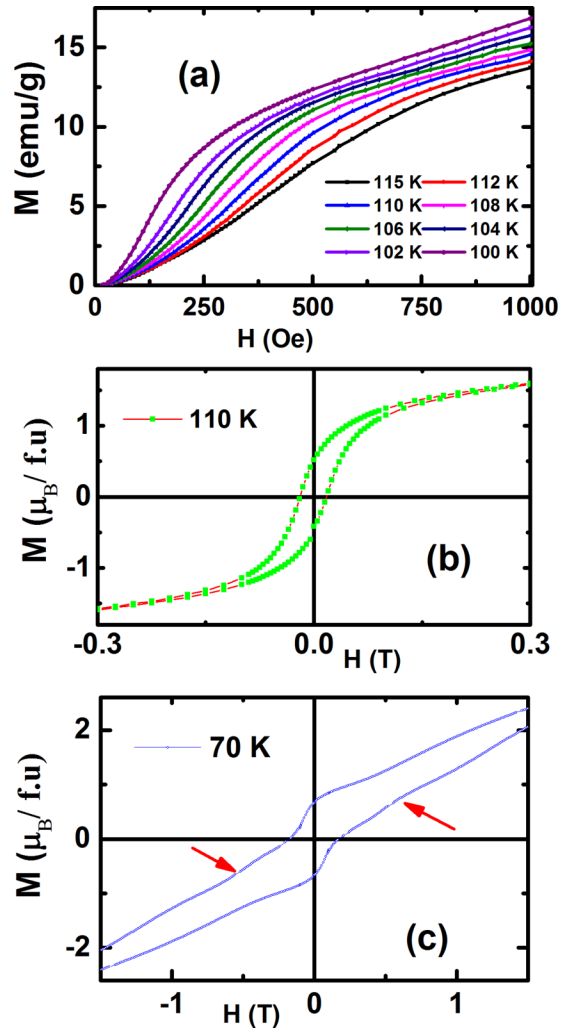

FIG. 5. (a) Low-field initial magnetization curves in the temperature range 100–115 K, whereas (b) shows the $M(H)$ hysteresis loop at 110 K and (c) for 70 K for GCMO. The red arrow indicates the weak metamagnetic nature of the material at low field at 70 K.

The data were collected in a stable mode in a small interval of magnetic field. We did not observe any characteristics of metamagnetism associated with first-order transition even at very low applied magnetic field in the temperature range 100–115 K [Fig. 5(a).] However, $M(H)$ curves show a weak hysteresis below 115 K. One representative plot is shown in Fig. 5(b) at 110 K, which reflects the typical behavior of a ferromagnet. Similar to previous reports, however, a weak metamagnetic behavior has been observed at low temperature as shown in Fig. 5(c) at 70 K as a representative [34,40]. Above 80 K, the anomaly is too weak to detect, though the FM loop sustains [see Fig. 5(b)]. We would like to mention that the anomaly associated with the metamagnetic transition in the present sample is much weaker as compared to that reported for a sample with smaller magnetic moment and lower T_C [34]. Clark *et al.* first reported the field-induced metamagnetic transition below 115 K in a polycrystalline GCMO sample and explained this phenomenon on the basis of a transition between uncompensated antiferromagnetic and ferromagnetic states below T_C [40]. However, in the single crystal, they

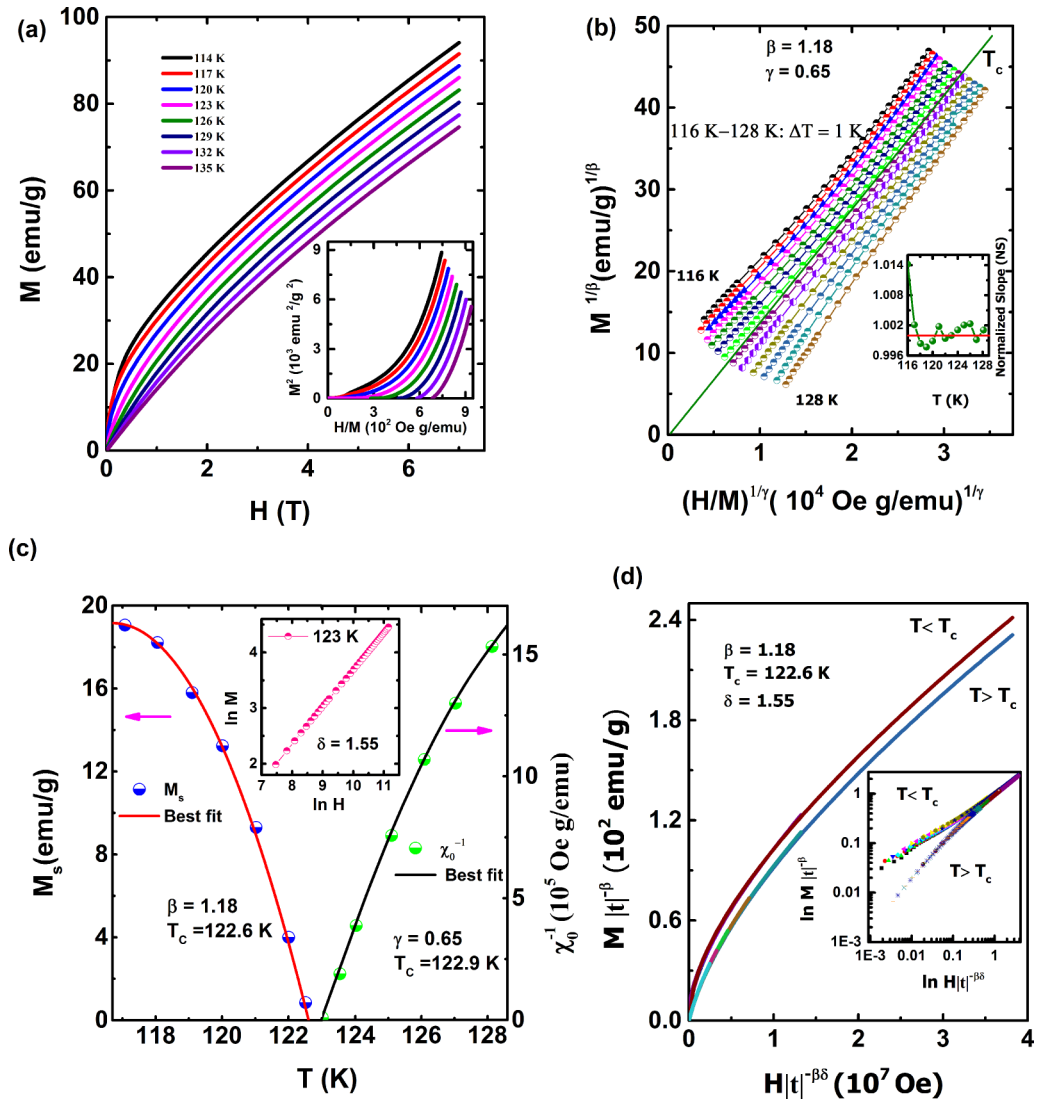

FIG. 6. (a) $M(H)$ isotherms of GCMO between 114 K (top) and 135 K (bottom) in 3 K interval (data with increasing field are shown). The lower inset shows the Arrott plot (M^2 vs H/M) of $M(H)$ isotherms. (b) Modified Arrott plot [$M^{1/\beta}$ vs $(H/M)^{1/\gamma}$] using $\beta = 1.18$ and $\gamma = 0.65$. The inset shows T dependence of normalized slope (NS). (c) Temperature dependence of spontaneous magnetization (M_S) and initial inverse susceptibility (χ_0^{-1}). The lines represent the best-fit curve according to Eqs. (3) and (4). The inset shows log-log plot of $M(H)$ isotherm for 123 K, the nearest one to the critical isotherm. (d) Scaling plots below and above T_C according to Eq. (7). The different symbols represent different temperatures. Inset shows the same plot in log-log scale.

did not observe a metamagnetic transition above 70 K [40]. Moon *et al.* also mentioned that, in their single crystal, the metamagnetic transition is absent above 100 K [31].

D. Critical behavior and scaling analysis

As there are no in-depth analyses of magnetic properties in GCMO such as critical behavior, etc., no consensus has been reached upon the nature of magnetic phase transitions in this system. The nature of FM to PM phase transition and the existence of GP-like clusters can also be studied through the detailed analysis of critical behavior. To investigate the critical behavior associated with FM transition, we have measured $M(H)$ isotherms in the temperature range 105 K $< T <$ 143 K and for fields up to 7 T. Few representative plots in the vicinity of T_C are shown in Fig. 6(a). We observe that, even at low field, M decreases monotonically with increase in temperature. This behavior is typical of a ferromagnet.

The $M(H)$ isotherms have been transformed into Arrott plots (M^2 versus H/M), which are shown in the lower inset of Fig. 6(a) [42]. The positive slope of the Arrott plots indicates that the FM transition is second order in nature [43]. In the vicinity of a second-order transition point, the diverging correlation length leads to the universal scaling laws for spontaneous magnetization (M_S), initial susceptibility (χ_0), and magnetization at T_C via a set of critical exponents β, γ, and δ, which are defined as [44,45]

$$M_S(0,t) \sim (-t)^{\beta}, \quad t < 0, \tag{3}$$

$$\chi_0{}^{-1}(0,t) \sim (t)^{\gamma}, \quad t > 0, \tag{4}$$

$$M(H,0) \sim (H)^{1/\delta}, \quad t = 0, \tag{5}$$

where $t = (T - T_C)/T_C$ is the reduced temperature. All three exponents β, γ, and δ are not independent of each other, rather they are related via the Widom scaling relation,

$$\delta = 1 + \frac{\gamma}{\beta}. \tag{6}$$

Furthermore, the field and temperature dependence of magnetization in the critical regime obeys a universal scaling relation of the form

$$M(H,t) = |t|^{\beta} f_{\pm}\left[\frac{H}{|t|^{(\beta\delta)}}\right], \tag{7}$$

where f_+ is for $t > 0$ and f_- is for $t < 0$.

To calculate the critical exponents and T_C, we use the modified Arrott plot (MAP) based on the Arrott-Noakes equation of state,

$$\left(\frac{H}{M}\right)^{1/\gamma} = at + bM^{1/\beta}, \tag{8}$$

where a and b are constants [44,45]. The MAP [Fig. 6(b)] shows almost parallel straight lines in the high field regime. During the least-squares fitting to the isotherms, the low-field data have been excluded because they represent mainly the rearrangement of magnetic domains. The convergence in the fitting is achieved for $\beta = 1.18$ and $\gamma = 0.65$. The obtained values of exponents are quite far from any conventional universality class.

Here, we would like to mention that, in several related double perovskite systems, magnetization is reported to follow conventional scaling behavior. La_2NiMnO_6 and Y_2NiMnO_6 obey scaling behavior belonging to 3D Heisenberg and 3D Ising class, respectively [46,47], while the values of critical exponents for Pr_2CoMnO_6 and Lu_2NiMnO_6 are close to that for mean field [29,48]. From Fig. 6(b), it is clear that an isotherm between 122 and 123 K will pass through the origin, suggesting T_C is very close to 122.5 K, consistent with T_C determined from the heat capacity data. To check whether the straight lines in Fig. 6(b) are parallel to each other, we have plotted the normalized slope $NS(T) = dM^{1/\beta}/d(H/M)^{1/\gamma}$ for different isotherms as shown in the inset of Fig. 6(b). The values of NS for different temperatures near T_C are close to 1, indicating that the isotherms in MAP are almost parallel to each other. The intersections of these isotherms for $T < T_C$ on $M^{1/\beta}$ axis and for $T > T_C$ on $(H/M)^{1/\gamma}$ axis give the values of M_S and χ_0^{-1}, respectively. The temperature dependence of M_S and χ_0^{-1} are shown in Fig. 6(c). The power-law fitting to M_S and χ_0^{-1} according to the Eqs. (3) and (4), respectively, reveals $\beta = 1.18 \pm 0.06$ with $T_C = 122.6 \pm 0.2$ K and $\gamma = 0.65 \pm 0.01$ with $T_C = 122.9 \pm 0.3$ K. Another exponent δ has been determined from the $M(H)$ curve at $T = 123$ K, the nearest one to the critical isotherm. The log-log plot of the $M(H)$ curve at $T = 123$ K gives $\delta = 1.55 \pm 0.03$ [Eq. (5)], which is shown in the inset of Fig. 6(c). With the obtained values of β, δ, and T_C, we have plotted the scaling relation $M|t|^{-\beta}$ vs $H|t|^{-\beta\delta}$, which is shown in Fig. 6(d). A similar plot of the scaling relation in log scale has been shown in the inset of Fig. 6(d). Depending on the sign of t, the magnetization data fall onto two branches of the curve. This suggests that the critical exponents and T_C are reasonably accurate. Moreover, one can see that the Widom scaling relation [Eq. (6)] is also satisfied [44]. It may be mentioned that the critical behavior of GCMO has also been analyzed after subtracting the Gd^{3+} moment ($\chi_{RE}H$) from the measured magnetization (not shown) and the critical exponents are found to be $\beta = 1.2$, $\gamma = 0.64$, and $\delta = 1.53$. Thus the change in the values of critical exponents is very small and within our experimental error.

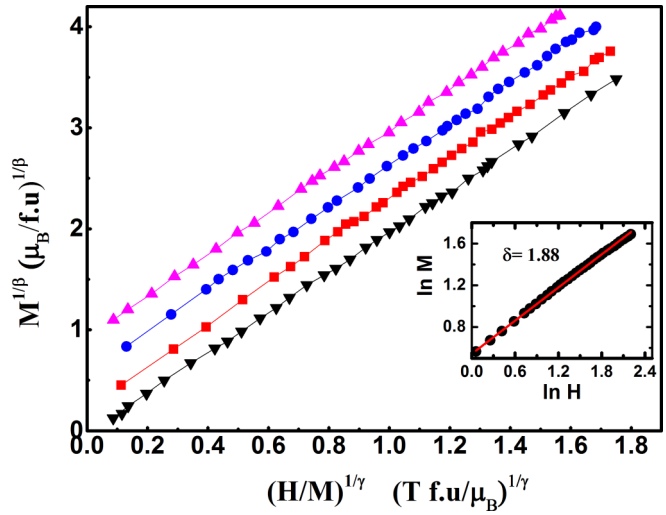

FIG. 7. Modified Arrott plot [$M^{1/\beta}$ vs $(H/M)^{1/\gamma}$] using $\beta = 1.88$ and $\gamma = 0.65$ of the easy-axis magnetization data of GCMO single crystal. The magnetization data were taken from Ref. [31]. The inset shows the log-log plot of $M(H)$ isotherm close to T_C.

In this work, the critical phenomenon has been studied on a polycrystalline GCMO sample. In an anisotropic compound, the polycrystalline nature of the sample may affect the scaling behavior. For systems with strong magnetic anisotropy, the magnetization along the easy axis exhibits critical phenomenon, whereas the hard axis can show noncritical behavior. In such cases, the noncritical magnetization along the hard axis becomes negligibly small and does not affect the analysis of critical behavior in the polycrystalline sample. Experimental studies on a GCMO single crystal reveal that the magnetic anisotropy in this system is strong [31]. We have analyzed the reported $M(H)$ isotherms along the magnetic easy axis as well as the hard axis of a GCMO single crystal in the vicinity of the FM transition [31]. The easy-axis magnetization is found to obey critical behavior similar to what we have observed in the polycrystalline sample, whereas the hard axis does not exhibit any critical behavior. Few $M(H)$ curves just below the T_C have been analyzed and observed that the $(H/M)^{1/\gamma}$ versus $M^{1/\beta}$ plot, as shown in Fig. 7, becomes linear for β and γ close to 1.18 and 0.65, respectively. We have also determined the exponent $\delta = 1.88$ from the log-log plot of $M(H)$ very close to T_C for applied field parallel to the easy axis of magnetization ($H \parallel c$), which is close to our polycrystalline data $\delta = 1.55$.

The critical exponent can also be determined through magnetocaloric analysis. The change in magnetic entropy (ΔS_m) has been calculated using the Maxwell relation [49]. The temperature dependence of ΔS_m for different magnetic fields is shown in Fig. 8(a). $\Delta S_m(T)$ exhibits a peak at T_C (~123 K). The maximum value of ΔS_m, $\Delta S_m^{\max}$, is observed to follow a

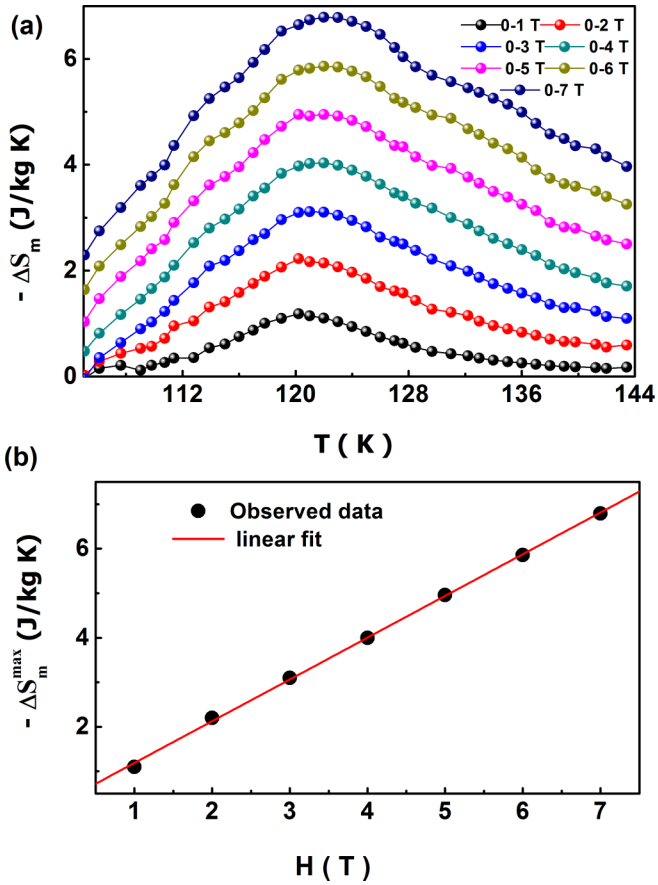

FIG. 8. (a) Temperature dependence of magnetic entropy change (ΔS_m) for different field change. (b) H dependence of maximum magnetic entropy change ($\Delta S_m^{\max}$). The solid line corresponds to linear fit.

power-law behavior [50]

$$\Delta S_m^{\max} \approx H^n. \tag{9}$$

We have plotted $\Delta S_m^{\max}$ as a function of field in Fig. 8(b). The figure shows that $\Delta S_m^{\max}$ increases almost linearly with H, which means n is close to 1. According to the Arrott-Noakes equation of state, n is related to critical exponents β and γ through the relation [50]

$$n = 1 + \frac{\beta - 1}{\beta + \gamma}. \tag{10}$$

Using the value of β and γ as calculated from the magnetization scaling analysis, we deduce $n = 1.09$, an excellent agreement with the above mentioned experimental value, indicating that the values of critical exponents are unambiguous and self-consistent.

In the case of GP, the conventional scaling theory breaks down due to the nonanalytical nature of magnetization. From the Yang-Lee theory of phase transition, one can derive an approximate magnetization scaling relation for phase transition from FM state to GP, which is given by [30]

$$\frac{M(h,t)}{\mu} = e^{-\left[\frac{A(t)}{\pi}\right]}\left[f_M\left(\frac{A(t)}{h}\right) + O(h)\right], \tag{11}$$

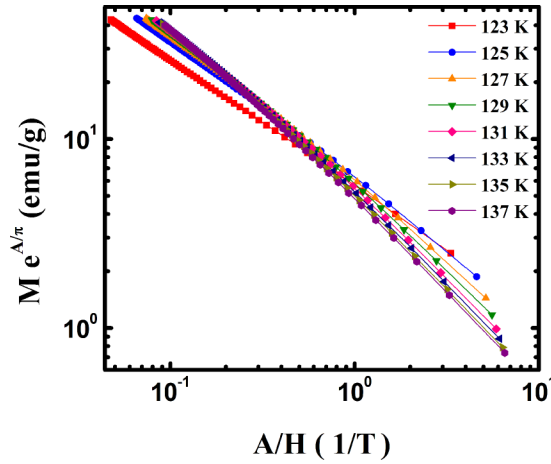

FIG. 9. Data collapse of magnetization $M(h,t)$ followed by Eq. (11) in logarithmic scale.

where

$$f_M(x) = -g_0 \mathrm{Im}[\exp(ix/2)E_1(ix/2)], \quad E_1(x) = \int_x^\infty \frac{e^{-t}}{t} dt.$$

μ is the magnetic moment of individual spin, $h = \mu H/k_B T_C$, and $A(t) = A_0 t^{2-\beta_r}$, where A_0 is constant and β_r is the order parameter exponent whose value reflects the universality class. Following Eq. (11), we have tried to collapse $M(H)$ isotherms of GCMO onto a single curve by plotting $M\, e^{A/\pi}$ versus A/H. By varying the parameters β_r and A_0, we have tried to achieve the convergence in fitting and the best scaling plot is obtained for $\beta_r = 1.8$ and $A_0 = 0.98$, which is shown in Fig. 9. It is clear from the figure that the data points can't be scaled at all, suggesting that GP does not exist in GCMO. It may be mentioned that the presence of GP in $La_{0.7}Ca_{0.3}MnO_3$ has been confirmed through such type of scaling analysis [21,22,30]. The asymptotic behavior of $M(h,t)$ in the Griffiths ferromagnet reveals [30]

$$M(h,t) \to \frac{\mu g_0 \pi}{2},$$

as h and A tend to zero. Thus there should be a discontinuity in $M(h,t)$, which is characterized by the large value of the exponent δ. Indeed, the critical exponent δ is found to be unusually large in several colossal magnetoresistive compounds due to the presence of GP [21,22,51]. On the contrary, the small value of δ in GCMO implies the non-Griffiths-like behavior of the clustered phase.

IV. CONCLUSION

In conclusion, we have studied the nature of the clustered phase, in double perovskite GCMO. The evolution of inverse susceptibility with temperature and external field are not consistent with the Griffiths phase. The non-Griffiths-like nature of the clusters has also been confirmed through the detailed analysis of the critical behavior. Furthermore, the calculated values of critical exponents β, γ, and δ associated to ferromagnetic to paramagnetic phase transition are far from any known existing universality class.

[1] H. J. Zhao, W. Ren, Y. Yang, J. Íñiguez, X. M. Chen, and L. Bellaiche, Nat. Commun. **5**, 4021 (2014).

[2] J. Meng, X. Liu, X. Hao, L. Zhang, F. Yao, J. Meng, and H. Zhang, Phys. Chem. Chem. Phys. **18**, 23613 (2016).

[3] J. Su, Z. Z. Yang, X. M. Lu, J. T. Zhang, L. Gu, C. J. Lu, Q. C. Li, J. M. Liu, and J. S. Zhu, Appl. Mater. Inter. **7**, 13260 (2015).

[4] H. S. Nair, D. Swain, N. Hariharan, S. Adiga, C. Narayana, and S. Elzabeth, J. Appl. Phys. **110**, 123919 (2011).

[5] P. N. Lekshmi and M. R. Varma, Mater. Sci. Forum **830-831**, 513 (2015).

[6] R. B. M. Filho, A. P. Ayala, and C. W. A. Paschoa, Appl. Phys. Lett. **102**, 192902 (2013).

[7] J. Blasco, J. García, G. Subías, J. Stankiewicz, J. A. Rodrguez-Velamazán, C. Ritter, J. L. García-Muñoz, and F. Fauth, Phys. Rev. B **93**, 214401 (2016).

[8] G. King and P. M. Woodward, J. Mater. Chem. **20**, 5785 (2010).

[9] R. N. Mahato, K. Sethupathi, and V. Sankaranarayanan, J. Appl. Phys. **107**, 09D714 (2010).

[10] N. S. Rogado, J. Li, A. W. Sleight, and M. A. Subramanian, Adv. Mater. **17**, 2225 (2005).

[11] L. Y. Wang, Q. Li, Y. Y. Gong, D. H. Wang, Q. Q. Cao, and Y. W. Du, J. Am. Ceram. Soc. **97**, 2024 (2014).

[12] H. Y. Zhou and X. M. Chen, J. Phys.: Condens. Matter **29**, 145701 (2017).

[13] J. K. Murthy, K. D. Chandrasekhar, S. Mahana, D. Topwal, and A. Venimadhav, J. Phys. D: Appl. Phys. **48**, 355001 (2015).

[14] A. K. Singh, S. Chauhan, S. K. Srivastava, and R. Chandra, Solid State Commun. **242**, 74 (2016).

[15] H. S. Nair, R. Pradheesh, Y. Xiao, D. Cherian, S. Elizabeth, T. Hansen, T. Chatterji, and Th. Bruckel, J. Appl. Phys. **116**, 123907 (2014).

[16] R. Masrour and A. Jabar, Chin. Phys. B **25**, 087502 (2016).

[17] J. Krishnamurthy and A. Venimadhav, *Magnetocaloric Effect in Double Pervoskite* La_2CoMnO_6, AIP Conf. Proc. No. 1447 (AIP, Melville, NY, 2012), p. 1235.

[18] M. Nasir, S. Kumar, N. Patra, D. Bhattacharya, S. N. Jha, D. R. Basaula, S. Bhatt, M. Khan, S. W. Liu, S. Biring, and S. Sen, ACS Appl. Electron. Mater. **1**, 141 (2019).

[19] M. Triki, E. Dhahri, and E. K. Hlil, J. Solid. State Chem. **201**, 63 (2013).

[20] D. Bhoi, N. Khan, A. Midya, M. Nandi, A. Hassen, P. Choudhury, and P. Mandal, J. Phys. Chem. C **117**, 16658 (2013).

[21] M. B. Salamon, P. Lin, and S. H. Chun, Phys. Rev. Lett. **88**, 197203 (2002).

[22] M. B. Salamon and S. H. Chun, Phys. Rev. B **68**, 014411 (2003).

[23] W. Jiang, X. Z. Zhou, G. Williams, Y. Mukovskii, and K. Glazyrin, Phys. Rev. B **77**, 064424 (2008).

[24] S. M. Zhou, Y. Li, Y. Q. Guo, J. Y. Zhao, X. Cai, and L. Shi, J. Appl. Phys. **114**, 163903 (2013).

[25] W. Liu, L. Shi, S. Zhou, J. Zhao, Y. Li, and Y. Guo, J. Appl. Phys. **116**, 193901 (2014).

[26] T. Chakraborty, H. S. Nair, H. Nhalil, K. R. Kumar, A. M. Strydom, and S. Elizabeth, J. Phys.: Condens. Matter **29**, 025804 (2017).

[27] R. R. Das, P. N. Lekshmi, S. C. Das, and P. N. Santhosh, J. Alloys Compd. **773**, 770 (2019).

[28] S. A. Ivanov, M. S. Andersson, J. Cedervall, E. Lewin, M. Sahlberg, G. V. Bazuev, P. Nordblad, and R. Mathieu, J. Mater. Sci.: Mater. Electron. **29**, 18581 (2018).

[29] L. Zhang, T. L. Shi, J. J. Cao, S. M. Yan, Y. Fang, Z. D. Han, B. Qian, X. F. Jiang, and D. H. Wang, J. Alloys Compd. **763**, 613 (2018).

[30] P. Y. Chan, N. Goldenfeld, and M. Salamon, Phys. Rev. Lett. **97**, 137201 (2006).

[31] J. Y. Moon, M. K. Kim, Y. J. Choi, and N. Lee, Sci. Rep. **7**, 16099 (2017).

[32] R. I. Dass and J. B. Goodenough, Phys. Rev. B **67**, 014401 (2003).

[33] M. Retuerto, A. Munoz, M. J. M. Lope, J. Alonso, F. J. Mompean, M. T. Fernandez, and J. S. Benitez, Inorg. Chem. **54**, 10890 (2015).

[34] J. Krishna Murthy and A. Venimadhav, J. Alloys Compd. **719**, 341 (2017).

[35] J. Y. Moon, M. K. Kim, D. G. Oh, J. H. Kim, H. J. Shin, Y. J. Choi, and N. Lee, Phys. Rev. B **98**, 174424 (2018).

[36] M. Das, S. Roy, N. Khan, and P. Mandal, Phys. Rev. B **98**, 104420 (2018).

[37] C. He, M. A. Torija, J. Wu, J. W. Lynn, H. Zheng, J. F. Mitchell, and C. Leighton, Phys. Rev. B **76**, 014401 (2007).

[38] R. C. Sahoo, S. Das, and T. K. Nath, J. Magn. Mater. **460**, 409 (2018).

[39] P. Mandal, A. Hassen, J. Hemberger, A. Krimmel, and A. Loidl, Phys. Rev. B **65**, 144506 (2002).

[40] A. Marsh and C. C. Clark, Philos. Mag. **19**, 449 (1969).

[41] X. L. Wang, J. Horvat, H. K. Liu, A. H. Li, and S. X. Dou, Solid State Commun. **118**, 27 (2001).

[42] A. Arrott and J. E. Noakes, Phys. Rev. Lett. **19**, 786 (1967).

[43] B. K. Banerjee, Phys. Lett. **12**, 16 (1964).

[44] N. Khan, A. Midya, K. Mydeen, P. Mandal, A. Loidl, and D. Prabhakaran, Phys. Rev. B **82**, 064422 (2010).

[45] H. Eugene Stanley, *Science (Introduction to Phase Transitions and Critical Phenomena)* (Oxford University Press, New York, 1971), Vol. 176, p. 502.

[46] X. Luo, B. Wang, Y. P. Sun, X. B. Zhu, and W. H. Song, J. Phys.: Condens. Matter **20**, 465211 (2008).

[47] H. Nhalil, H. S. Nair, and S. Elizabeth, *Critical Behavior of* Y_2NiMnO_6 *Double Perovskite*, AIP Conf. Proc. No. 1728 (AIP, Melville, NY, 2016), p. 020184.

[48] I. N. Bhattia, R. N. Mahatob, I. N. Bhatti, and M. A. H. Ahsan, Phys. B: Condens. Matter **558**, 59 (2019).

[49] V. K. Pecharsky and K. A. Gschneidner, Jr., Phys. Rev. Lett. **78**, 4494 (1997).

[50] V. Franco, J. S. Blazquez, and A. Condea, Appl. Phys. Lett. **89**, 222512 (2006).

[51] W. Jiang, X. Z. Zhou, G. Williams, Y. Mukovskii, and K. Glazyrin, Phys. Rev. Lett. **99**, 177203 (2007).